Feedback Coupling and Early Detection of Thermoacoustic Combustion Instability

Yosuke Mori, Sena Kishiya, Takuya Kurosaka, and Hiroshi Gotoda[*]

*Department of Mechanical Engineering, Tokyo University of Science, 6-3-1 Niijuku, Katsushika-ku, Tokyo
125-8585, Japan*

We study the feedback coupling of thermoacoustic combustion instability from the viewpoint of a complex-systems approach, including the early detection of combustion instability. An upwardly traveling large-scale transverse vortex motion gives rise to large heat release rate fluctuations in the shear layer region between the inner and outer recirculation flows. The directional coupling from flow velocity to heat release rate fluctuations clearly appears near the rolled-up flame front generated by the developed transverse vortical structure. These events are strongly associated with the formation of a strong and local thermoacoustic power source cluster during combustion instability. A methodology combining symbolic dynamics-based analysis and a convolutional neural network enables the detection of a precursor of combustion instability.

I. INTRODUCTION

A feedback coupling among fluctuations in acoustic pressure, heat release rate, and flow velocity fields results in the onset of large-amplitude acoustic oscillations in a confined combustor, collectively called thermoacoustic combustion instability [1]. The emergence of such an instability structurally damages the combustor through the enhanced heat transfer and mechanical vibrations. An understanding of the physical mechanism of the feedback coupling and an early detection of combustion instability have been an ongoing scientific pursuit and challenge that stimulated the current interest in the development of industrial combustors for thermal power generation and aerospace propulsion systems.

A complex-systems approach based on the framework of synchronization and network science is on track to significantly broaden our understanding of the nonlinear dynamics of combustion instability in various turbulent combustors [2–5]. Recent experimental studies [6–9] have examined the mutual interplay between acoustic pressure and heat release rate fluctuations from the viewpoint of a complex-systems approach. Pawar *et al.* [6] have shown that a combustion state undergoes a transition from the desynchronized aperiodic state (stable combustion) to the phase-synchronized state (combustion instability). Godavarthi *et al.* [8] have conducted a subsequent study on the clarification of the directional dependence of desynchronized/synchronized states.

Symbolic dynamics-based analysis in terms of permutation (ordinal) patterns in a time series has opened new avenues to understanding various dynamic behaviors that emerge in nonlinear systems [10]. Many experimental studies [11–15] have examined the randomness of acoustic pressure fluctuations during stable combustion and combustion instability by quantifying permutation entropy [16] and the missing pattern numbers of acoustic pressure fluctuations. Small and coworkers [17,18] have proposed an ordinal pattern-based transition network incorporating the permutation patterns in a time series. The transition network entropy has been shown to be an effective measure to capture significant changes in combustion state in two model combustors: a model gas-turbine combustor [19] and a model rocket engine combustor [20]. Asami *et al.* [21] have shown that the symbolic recurrence rate [22] for evaluating the synchronized state between the acoustic pressure and heat release rate fluctuations enables the capture of a precursor of combustion instability in a swirl-stabilized turbulent combustor.

A statistical learning theory has recently been expected as one of the promising approaches to developing sophisticated early detectors of combustion instability [23–25]. Hachijo *et al.* [23] have attempted to detect combustion instability in a swirl-stabilized turbulent combustor using a methodology combining the complexity-entropy causality plane [26] and a support vector machine (SVM) [27,28]. Recurrence quantification analysis in combination with the SVM has been adopted for a staged multisector combustor [24] and a liquid rocket engine [25]. The construction and progress of various detection methodologies incorporating machine learning technology are desired in

---

[*]Corresponding author:gotoda@rs.tus.ac.jp

current nonlinear science and related branches of applied physics.

This study aims to experimentally conduct an intensive study of (i) the physical mechanism on the feedback coupling among acoustic pressure, heat release rate, and flow velocity fluctuations during combustion instability and (ii) the applicability of symbolic dynamics-based detection methodology in combination with deep learning to capture a precursor of combustion instability. We address the combustion dynamics in a swirl-stabilized turbulent combustor as an important case study related to fundamental and practical combustion systems. Hashimoto *et al.* [29] have proposed a phase parameter for evaluating the degree of coherent state in the phase field constructed from acoustic pressure and heat release rate fluctuations in a model rocket combustor. They have also shown that the directionality index estimated from transfer entropy is valid for examining the mutual coupling between the two fluctuations in the model rocket combustor. On this basis, we propose a new causality index combining information theory, synchronization, and complex networks, to clarify the feedback coupling mechanism during combustion instability. Kobayashi *et al.* [19] and Asami *et al.* [21] have recently shown that multivariate ordinal pattern-based transition network entropy [30] and symbolic recurrence rate [22] are useful for dealing with dynamic behavior interacting between acoustic pressure and heat release rate fluctuations. A convolutional neural network (CNN) is one of the deep learning methods widely applied in the field of image recognition [31,32]. Ruiz *et al.* [33] have attempted to predict the onset of combustion instability in a bluff-body combustor using a recurrence network in combination with a CNN. Based on recent studies [19,21,33], we propose a novel early detection methodology for combustion instability by adapting a CNN to symbolic recurrence plots (SRPs) in this study.

This paper is organized into four sections. Brief descriptions of the experiments and analytical methods are provided in Secs. II and III, respectively. The results and discussion are presented in Sec. IV, and a summary of this study is given in Sec. V.

II. EXPERIMENTS

Figure 1 shows a schematic of a swirl-stabilized turbulent combustor [34] and measurement system used in this study. Note that our combustion test rig consists of electronic mass flow controllers, a venturi mixer, a nozzle, an axial swirler, and a combustion chamber with a water-cooled duct. The fuel and air flow rates are adjusted by the mass flow controllers. The regulated fuel and air are injected into the venturi mixer to form a homogeneous premixture. The perfectly homogeneous premixture enters the combustion chamber through the nozzle and the swirler. We conduct the simultaneous measurements of acoustic pressure, OH* chemiluminescence emission intensity, and flow velocity fluctuations inside the combustor. Note that OH* chemiluminescence emission intensity represents the heat release rate produced by a premixed turbulent flame. Acoustic pressure fluctuations p' are acquired using a water-cooled pressure transducer (JTEKT Products, PD104K-10kPa) placed on the side wall of the combustor. The OH* chemiluminescence emission intensity images are acquired using a high-speed camera (Photron, FASTCAM SA-3) with an image intensifier (Hamamatsu Photonics, C9548-03), a UV lens (Nikon, UV-105mm F4.5), and an OH* band-pass filter (ASAHI SPECTRA Co., MZ0310). The measurement region of the OH* chemiluminescence emission intensity fluctuations I' is 48 mm × 90 mm with a resolution of 0.14 mm/pixel for the left-hand side of the combustor. We also measure
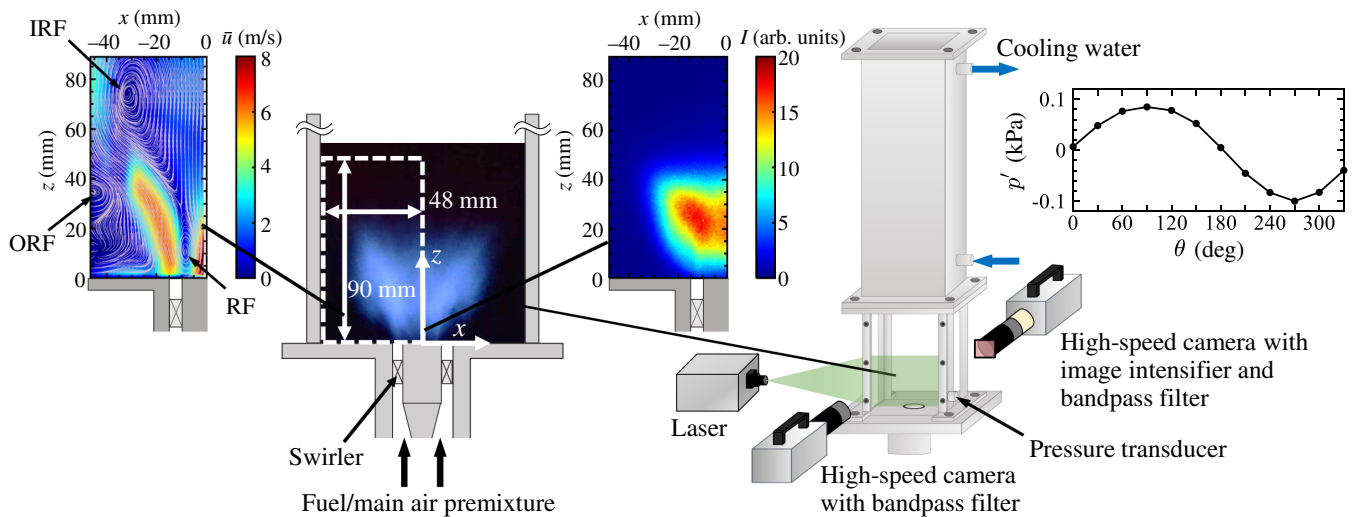

FIG. 1.   Experimental system.

I' in the region of 100 mm × 100 mm using a photomultiplier (Hamamatsu Photonics, H10722-210) with the same band-pass filter (ASAHI SPECTRA Co., MZ0310). The former I' obtained using the high-speed camera is used for elucidating the feedback mechanism during combustion instability, whereas the latter obtained using the photomultiplier is used for an early detection of combustion instability by symbolic dynamics-based analysis in combination with deep learning. The sampling frequencies of p' and I' are both 6 kHz. We obtain the two-dimensional flow velocity field u ($= \sqrt{u_x^2 + u_z^2}$, where u_x and u_z are the flow velocities in the x and z direction, respectively) by particle image velocimetry and using a DaVis system (LaVision GmbH, version 8.4.1) [34]. A diode-pumped solid-state laser (LaserQUANTUM, Finesse 532 nm) with a maximum output of 10 W is used as a continuous light source, and the thickness of the laser sheet is approximately 1.0 mm. The Mie scattered light from the particles in the premixture is obtained using a high-speed camera (Photron, FASTCAM SA-Z) equipped with a UV lens and a band-pass filter (LaVision, VZ-Image Filter). The measurement region of the flow velocity field is the same as that of the OH* chemiluminescence emission intensity, namely, 48 mm × 90 mm with a resolution of 0.12 mm/pixel. The sampling frequency of flow velocity fluctuations u' is 60 kHz. The mean axial flow velocity and the swirl number of the CH_4/air premixture at the inlet of the combustor are set to 5.0 m/s and 0.70, respectively. The equivalence ratio of the premixture ϕ is increased from 0.65 to 0.80 so that the combustion state changes from stable combustion to well-developed combustion instability. The thermal power corresponding to these conditions ranges from 4.7 to 5.8 kW.

As reported in our recent paper [34], an inner recirculation flow (IRF), an outer recirculation flow (ORF) in the dump region, and a recirculation flow in the wake of the center body (RF) are formed inside the combustor during combustion instability. The entire flame is maintained through these recirculation flows. Large-scale vortical structures are observed in the shear layer region between the IRF and the ORF.

III. ANALYTICAL METHODS

The analytical methods involving spatial network, thermoacoustic power network, turbulence network, and a symbolic dynamics-based analysis in combination with a CNN are described as follows.

A. Spatial network

A spatial network using the two-point correlation of the spatial grid points of the observation domain is one of the simplest complex networks. Recent studies [35,36] have shown the applicability of the spatial network to clarifying the dynamics of turbulent flows. They have used

un unweighted spatial network based on a correlation-threshold approach. The spatial correlation between heat release rate and flow velocity fluctuations contributes to the understanding of the mutual coupling that is strongly associated with the driving mechanism of combustion instability. In this study, we use a weighted spatial network constructed from OH* chemiluminescence emission intensity and flow velocity fluctuations. The weighted spatial network comprises nodes corresponding to spatial locations of I' and u', and links representing the strength of the correlation between their temporal evolutions at two spatial locations inside the combustor. The adjacency matrix with a component $A_{s,ij}$ is given as (the links are given as the average absolute value of the correlation coefficient C_{ij} between I' and u' in each grid)

$$A_{s,ij} = \begin{cases} \frac{1}{2}\left(|C_{ij}| + |C_{ji}|\right) & \text{if } i \neq j \\ 0 & \text{otherwise } i = j \end{cases} \quad (1)$$

$$C_{ij} = \frac{\mathbb{E}\left[I'_j, u'_i\right]}{\sigma_{I'_j}\sigma_{u'_i}}. \quad (2)$$

Here, $\mathbb{E}\left[I'_j, u'_i\right]$ denotes the covariance between I'_j and u'_i; $\sigma_{I'_j}$ and $\sigma_{u'_i}$ denote the standard deviations of I'_j and u'_i, respectively. We obtain the vertex strength $s_{s,i}$ in the network as $s_{s,i} = \sum_{j=1}^{N} A_{s,ij}$. Note that the total number of nodes in the network N is set to 1104 in this study.

B. Thermoacoustic power network

A thermoacoustic power network, which is constructed from the product of acoustic pressure and heat release rate fluctuations, has been shown to be a useful complex network for inferring the driving region of combustion instability in a bluff-body turbulent combustor [37] and a model rocket combustor [38]. One important point obtained with this network is that the emergence of a coherent structure of thermoacoustic power plays an important role in the driving of combustion instability. In this study, we examine how the thermoacoustic cluster is formed during combustion instability using the thermoacoustic power network that enables a deepening of the understanding toward the coherent structure of acoustic energy. For the construction of the network, if the product of p' and I' at a spatial location (node) i, denoted as $p'_i I'_i$, and the same physical quantity at a spatial location j, denoted as $p'_j I'_j$, both take positive values, the nodes i and j are linked as the averages of $p'_i I'_i$ and $p'_j I'_j$. The thermoacoustic power network A_{ij} is given as

$$A_{a,ij} = \begin{cases} \frac{1}{2}(p'_i I'_i + p'_j I'_j) & \text{if } (i \neq j, \ p'_i I'_i > 0 \text{ and } p'_j I'_j > 0) \\ 0 & \text{otherwise.} \end{cases}$$

$$(3)$$

Here, acoustic energy propagates radially with sound speed inside the combustor. We infer that the propagation time of acoustic energy is shorter than the sampling period of p' and I' measurements (=1/6000 s). Based on this point and the implication of the Rayleigh index, we consider the connection between the nodes at two spatially distantly separated locations.

We estimate the cluster coefficient c_i in a node i and the average cluster coefficient $\langle c \rangle$ $(= 1/N \sum_{i=1}^{N} c_i$, where N is the total number of nodes in the network) in accordance with the definition of the cluster coefficient by Holme *et al.* [39]:

$$c_i = \frac{\sum_{j=1}^{N} \sum_{k=1}^{N} A_{a,ij} A_{a,jk} A_{a,ki}}{\max(\mathbf{A_a}) \sum_{j=1}^{N} \sum_{k=1}^{N} A_{a,ij} A_{a,ki}}. \quad (4)$$

Here, $\mathbf{A}_a$ is the adjacency matrix in the network. We obtain the vertex strength $s_{a,i} (= \sum_{j=1}^{N} A_{a,ij})$ in the network. Note that N is set to 8704 in this study.

C. Turbulence network

A turbulence network [40], which is constructed from the induced velocity in the flow field, has been adopted for examining the spatiotemporal dynamics of a flow velocity field during combustion instability [29,41–43]. The motion of the primary hub in the network based on vortical interactions is significantly associated with the driving mechanism of combustion instability. On this basis, we use the turbulence network in this study. It consists of the adjacency matrix defined as

$$A_{t,ij} = \begin{cases} \frac{1}{2}(v_{ij} + v_{ji}) & \text{if } i \neq j \\ 0 & \text{otherwise } i = j \end{cases} \quad (5)$$

$$v_{ij} = \frac{|\Omega(\mathbf{x}_i) \Delta x \Delta z|}{2\pi |\mathbf{x}_i - \mathbf{x}_j|}, \quad (6)$$

where v_{ij} is the induced velocity from fluid element i on another element j in the flow field, $\Omega(\mathbf{x}_i)$ is the vorticity at location $\mathbf{x}_i$, and Δx and Δz are the cell sizes of the vorticity field. Note that Δx and Δz are both 2 mm.

The Louvain method [44] is a standard method of community identification in a complex network based on modularity optimization. We extract the community structure in the turbulence network by the Louvain method to maximize the accuracy of community division. In this method, each node in the turbulence network is considered to belong to its own community and is aggregated into neighboring communities which maximizes the gain of modularity [44]. We use the module degree Z_i [45] for

the classification of characteristic nodes. Here Z_i evaluates how a node i is strongly connected to other nodes in a community. Similarly to a previous study [45], we classify nodes with $Z_i \geq 2.5$ as module hubs.

D. Causality analysis

We introduce a new causality index, which combines synchronization, complex network, and information theory, namely, spatial-network-based transfer entropy, to deal with the feedback coupling between I' and u'. Based on the concept of phase parameter [29] in terms of a spatially coherent state during combustion instability, we first construct the adjacency matrices for I' and u' denoted as $A_{I',ij}$ and $A_{u',ij}$, respectively.

$$A_{I',ij} = \begin{cases} 1 & \text{if } \cos\theta_{I'} > \cos\theta_{\text{th}}, \\ 0 & \text{otherwise}. \end{cases} \quad (7)$$

Here, $A_{I',ij}$ is the adjacency matrix for I' at a time and $\theta_{I'}$ is the phase difference between the instantaneous phases of ith and jth points of I' at a time. The instantaneous phase is obtained by Hilbert transformation [41,46]. Note that $\cos\theta_{\text{th}}$ is set to 0.9 in this study. The nodes are linked when the phase difference between them is small. Their connection means the formation of coherent structure.

Based on the concept of transfer entropy [47], we here consider the information flow between $A_{I',ij}$ and $A_{u',ij}$. The causality of u' and I' at each time can be estimated as (an important point in this methodology is that $E_{T,I'\to u'}$ increases as the relative information transport from I' to u' becomes predominant)

$$E_{T,I'\to u'} = \sum_{a_1,a_2,a_3=0}^{1} P\left(u'(t_k), u'(t_{k+1}), I'(t_k)\right)$$
$$\times \log_2 \frac{P\left(u'(t_{k+1}) \mid u'(t_k), I'(t_k)\right)}{P\left(u'(t_{k+1}) \mid u'(t_k)\right)} \quad (8)$$

$$P\left(u'(t_k), u'(t_{k+1}), I'(t_k)\right)$$
$$= \frac{1}{N} \sum_{i,j=1}^{N} \chi_1\left(A_{u',ij}(t_k)\right) \chi_2\left(A_{u',ij}(t_{k+1})\right) \chi_3\left(A_{I',ij}(t_k)\right) \quad (9)$$

$$P\left(u'(t_{k+1}) \mid u'(t_k), I'(t_k)\right)$$
$$= \frac{\sum_{i,j=1}^{N} \chi_1\left(A_{u',ij}(t_k)\right) \chi_2\left(A_{u',ij}(t_{k+1})\right) \chi_3\left(A_{I',ij}(t_k)\right)}{\sum_{i,j=1}^{N} \chi_1\left(A_{u',ij}(t_k)\right) \chi_3\left(A_{I',ij}(t_k)\right)} \quad (10)$$

$$P\left(u'(t_{k+1}) \mid u'(t_k)\right)$$

$$= \frac{\sum_{i,j=1}^{N} \chi_1\left(A_{u',ij}(t_k)\right)\chi_2\left(A_{u',ij}(t_{k+1})\right)}{\sum_{i,j=1}^{N} \chi_1\left(A_{u',ij}(t_k)\right)} \quad (11)$$

$$\chi_l(A_{ij}) = \begin{cases} 1 & \text{if } A_{ij} = a_l \\ 0 & \text{otherwise} \end{cases} \quad (12)$$

Here, $E_{T,I'\to u'}$ is a spatial-network-based transfer entropy for the direction from I' to u', $P(u'(t_k), u'(t_{k+1}), I'(t_k))$ is the joint probability of $u'(t_{k+1})$, $u'(t_k)$, and $I'(t_k)$, and $P(u'(t_{k+1})|u'(t_k))$ is the conditional probability of $u'(t_{k+1})$ given $u'(t_k)$. Note that N is set to 1104 in this study.

E. Symbolic dynamics-based detection method in combination with deep learning

SRPs enable us to evaluate the similarity between two simultaneously observed dynamic behaviors [22]. In this study, we introduce the SRPs consisting of p' and I' to develop a new detection methodology for combustion instability. For the construction of SRPs, we first extract time series data points D of p' and I' for each delay time τ_e according to the Bandt-Pompe concept [16], and classify them into $D!$ permutation patterns. If the permutation pattern of p' at t_i, denoted as $\pi_{p'}(t_i)$, and $\pi_{I'}(t_j)$ at time t_j are the same, a color plot corresponding to each pattern is given in SRPs:

$$S_{R,ij} = \begin{cases} 1 & \text{if } \pi_{p'}(t_i) = \pi_{I'}(t_j), \\ 0 & \text{otherwise.} \end{cases} \quad (13)$$

Note that D and τ_e are set to 5 and 1 (≈ 1.67 ms) in this study, respectively.

We estimate the symbolic recurrence rate [48] R_{SR} representing the density of SRPs. Here R_{SR} is defined as

$$R_{SR} = \frac{\sum_{i=1}^{N-\tau_e(D-1)-|\tau'|} S_{R,ij}}{N - \tau_e(D-1) - |\tau'|}. \quad (14)$$

Here, $j = i + \tau'$, N is the total number of data points in p' and I', and τ' specifies the time distance between the main diagonal line ($i = j$) and the parallel diagonal line in SRPs. Note that $N = 600$ and $\tau' = 0$ in this study. Here R_{SR} approaches unity if p' and I' exhibit similar behaviors.

We also estimate the ordinal pattern-based transition network entropy [30]. Similarly to the construction of SRPs, each of p' and I' is converted into a permutation pattern. After classifying the combination of permutation patterns of p' and I' into $\Pi = \{\Pi_i | i = 1, 2, \ldots, D!^2\}$, we calculate the transition probability $W_{ij} = P(\Pi_i \to \Pi_j)$,

where P is the existing probability from Π_i to Π_j. Here W_{ij} corresponds to a component in the adjacency matrix in the transition network, where $\sum_{i,j=1}^{D!^2} W_{ij} = 1$. The transition network entropy H_t is obtained by applying the transition probability distribution to the information entropy:

$$H_t = \frac{-\sum_{i,j=1}^{D!^2} W_{ij} \log_2 W_{ij}}{\log_2 D!^4}. \quad (15)$$

Note that H_t increases with the randomness of the network structure, where H_t ranges from zero to unity, and D and τ_e are set to 2 and 1 in this study, respectively.

The CNN consists of an input layer, a convolutional layer, a pooling layer, a fully connected layer, and an output layer [32,33]. Multiple convolutional and pooling layers are arranged to extract features from the input image. The extracted features are identified through the fully connected layer and the output layer, where the images are classified into each class. We first cluster the data sets $\{\mathbf{x}_i | i = 1, 2, \ldots, n\}$ for the implementation of the CNN. Note that $\mathbf{x}_i = (H_t, R_{SR})$ and $n = 4800$ in this study. The k-means method [28] is applied to classifying the combustion state into (i) stable combustion, (ii) the transitional state from stable combustion to combustion instability, and (iii) combustion instability. SRPs corresponding to $\mathbf{x}_i$ clustered by the k-means method are divided into two parts: the training data of the CNN and the validation data. The SRPs of the validation data are used to calculate the classification accuracy of the CNN.

Figure 2 shows the structure of the CNN employed in this study. We build a convolutional layer applying a small image (filter) to the input image and extract the features of the input image from those of the filter. Let one consider each pixel value of the input image as $S_{R,ij}$ ($i, j = 1, \ldots, N - (D-1)\tau_e$), each pixel value of the filter as h_{mn} ($m, n = 0, \ldots, H - 1$), and each element a_{ij} obtained from $S_{R,ij}$ and h_{mn} as

$$a_{ij} = \sum_{m=0}^{H-1}\sum_{n=0}^{H-1} S_{R,(i+m)(j+n)} h_{mn} + b. \quad (16)$$

Here, b represents the bias. The adaptive position of the filter is calculated by sliding the filter for each stride s. We set $H = 3$ and $s = 1$ in the convolutional layer. The convoluted values are given by an activation function, and the output is a feature map. In this study, we use a function f (rectified linear unit) [49]. The feature maps created in the convolutional layer serve as the input for the pooling layer. We use the max pooling method, in which only the maximum value is selected for the region to be extracted. The new feature map d can be expressed as
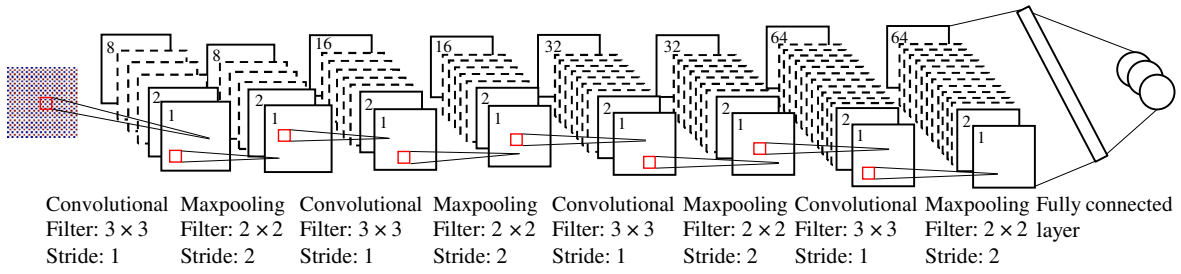
Convolutional	Maxpooling	Convolutional	Maxpooling	Convolutional	Maxpooling	Convolutional	Maxpooling	Fully connected
Filter: 3×3	Filter: 2×2	Filter: 3×3	Filter: 2×2	Filter: 3×3	Filter: 2×2	Filter: 3×3	Filter: 2×2	layer
Stride: 1	Stride: 2	Stride: 1	Stride: 2	Stride: 1	Stride: 2	Stride: 1	Stride: 2	

FIG. 2. Schematic of a convolutional neural network.

$d_{ij} = \max(f(a_{(i+m)(j+n)}))$. We set H and s to 2 in the pooling layer. In the fully connected layer, the feature maps are converted into one-dimensional arrays as input, and the feature vectors are obtained by multiplying the weights and adding the biases. In the output layer, which consists of the fully connected layer and the activation function, the obtained feature vectors are classified into k classes by the output layer. In the output layer, the softmax function is used to calculate the probability of each cluster. The class with the maximum probability will be output as the classification class of the input image. The filter values, weights, and biases are optimized by the backpropagation method [50] while training the CNN. The image features are extracted using four convolutional layers, four pooling layers, and an output layer consisting of a fully-connected layer and softmax function. We attempt to detect a precursor of combustion instability by classifying the images using a trained CNN.

IV. RESULTS AND DISCUSSION

Figure 3 shows the variation in the directionality index ΔS_T as a function of equivalence ratio ϕ. Note that the definition of $\Delta S_T (= S_{T,p' \to I'} - S_{T,I' \to p'}$, where S_T is the original version of the transfer entropy [47]) is the same as that used in a previous study [29] and ΔS_T is positive when the relative information transport from p' to I' is predominant. We clearly observe that ΔS_T is less than zero at $\phi = 0.65$ and monotonically increases with ϕ up to 0.76. This indicates that the relative information transport from heat release rate to acoustic pressure fluctuations predominates during stable combustion and the subsequent transitional state to combustion instability. In contrast, the sign of ΔS_T becomes positive when ϕ exceeds 0.77. This implies that the sufficiently amplified pressure fluctuations become relatively more predominant than the heat release rate fluctuations during well-developed combustion instability. Note that in our preliminary test, the change in ΔS_T in terms of ϕ is similar to that of the root mean square of p', but the root mean square can hardly clarify the switching of the causality relationship between acoustic pressure and heat release rate fluctuations during a transition to combustion instability.

Figure 4(a) shows the two-dimensional plane of the transition network entropy H_t and the symbolic recurrence rate R_{SR} obtained from the data sets. Here, H_t and R_{SR} are estimated for segments of p' and I' with $L = 0.1$ s at each ϕ. Note that p' and I' during 30 s are used in this study, where the number of data points for each ϕ is 300 ($= 30/0.1$). As ϕ increases, the location of (H_t, R_{SR}) moves from the lower right-hand side to the upper left-hand side on the $H_t - R_{SR}$ plane. The $H_t - R_{SR}$ plane captures the change in combustion state from stable combustion to combustion instability with increasing ϕ. The plane clustered into three regions by the k-means method [i.e. stable combustion (blue), the transitional state from stable combustion to combustion instability (yellow), and combustion instability (red)] is shown in Fig. 4(b), together with the SRPs extracted as a representative time in the three regions. The number of SRPs increases with the advent of combustion instability, observing the appearance of diagonal lines. The classification accuracy of SRPs images is 98% in this work. Figure 5 shows the classification of p' and I obtained from the test data using the trained CNN. Here, SRPs are constructed every $L = 0.1$ s from p' and I' obtained from the test data. Stable combustion continues at $t < 18.4$ s. Stable combustion and the transitional state are alternately formed at
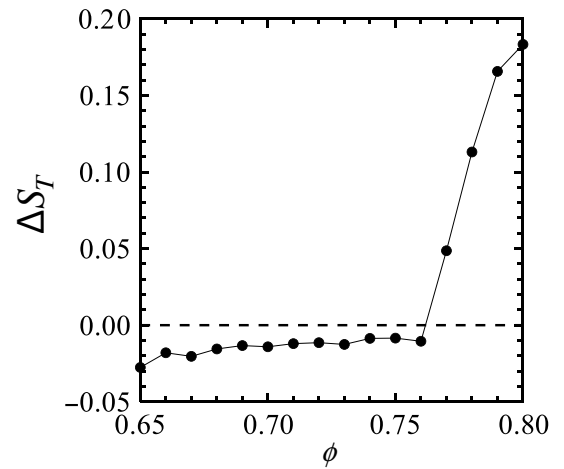
FIG. 3. Variation in the directionality index ΔS_T as a function of equivalence ratio ϕ.
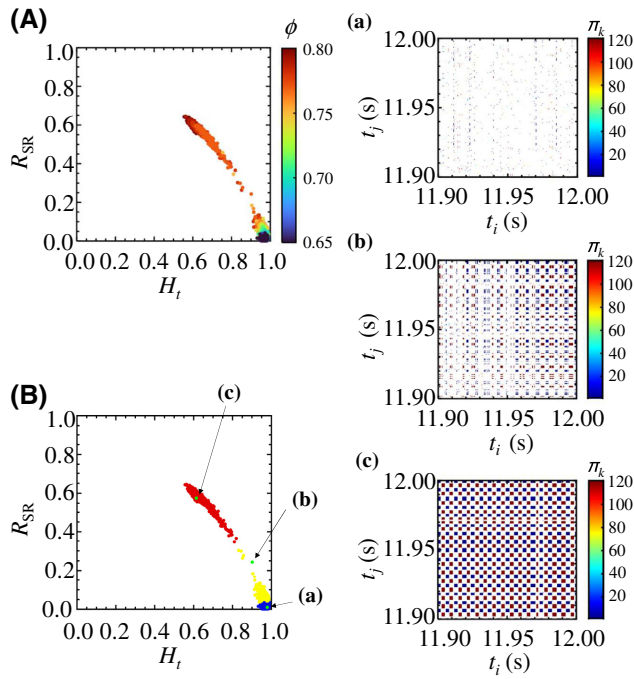
FIG. 4. (A) Two-dimensional plane of the transition network entropy H_t and the symbolic recurrence rate R_{SR} obtained from the data sets. (B) Classification of combustion states on $H_t - R_{SR}$ plane obtained by the k-means method. Here, (a) $\phi = 0.65$, (b) $\phi = 0.77$, and (c) $\phi = 0.8$.

18.4 s $\leq t \leq$ 32.6 s. Combustion instability is observable at $t \geq$ 32.7 s. The SRPs corresponding to $t = 11.1$ s, 29.0 s, and 42.1 s are classified into stable combustion, the transitional state, and combustion instability, respectively. The diagonal lines in SRPs increases toward the onset of combustion instability, which indicates that the trained CNN can appropriately capture the features of SRPs corresponding to the three regions. Shinchi *et al.* [24] have reported that a precursor of combustion instability is detected when the ratio of the formation duration of the transitional state to that of stable combustion exceeds 25%. In accordance with their report [24], the detection time of a precursor of combustion instability is estimated as $t = 29.9$ s. An important point to emphasize here is that the value of ϕ for the detection time corresponds to that in Fig. 3. This means that the switching of the causality relationship between acoustic pressure and heat release rate fluctuations plays an important role in an early detection of combustion instability. As stated in Sec. I, many experimental studies [23–25,51] on an early detection of combustion instability have clearly shown the importance of the SVM for determining the boundary between combustion states in various thermoacoustic combustion systems. In our preliminary test applying the SVM to the $H_t - R_{SR}$ plane, the detection time obtained by our methodology almost coincides with that obtained by the SVM, although the comparison of the detection time between the CNN and the SVM should be

examined in a broad range of the rates in increase in the equivalence ratio in terms of time.

In this study, we have used the SRPs, which enables the visualization of the mutual interaction between acoustic pressure and heat release rate fluctuations, as images to train the CNN. The trained CNN can find a precursor of combustion instability that is difficult to discern from the long-term average of p' and I'. The CNN possesses a detection accuracy equivalent to that of the SVM and can incorporate transfer learning that is applicable to other combustors, although one needs in advance the data sets for training the CNN. Thus far, various types of recurrences plots such as the cross recurrence and the joint recurrence plots [22] have been proposed. These recurrence plots including the original version of the recurrence plots [52] require the appropriate setting of the radius of the hypersphere in the phase space. The geometrical structures in these plots depend strongly on the radius threshold. They also need the computation of Euclidean distances between the points in the phase space. The main advantages of the SRPs compared with the above recurrence plots as the input image for the CNN are that one can reduce the dependence of parameters for the construction of the recurrence plots and computational cost. This is very
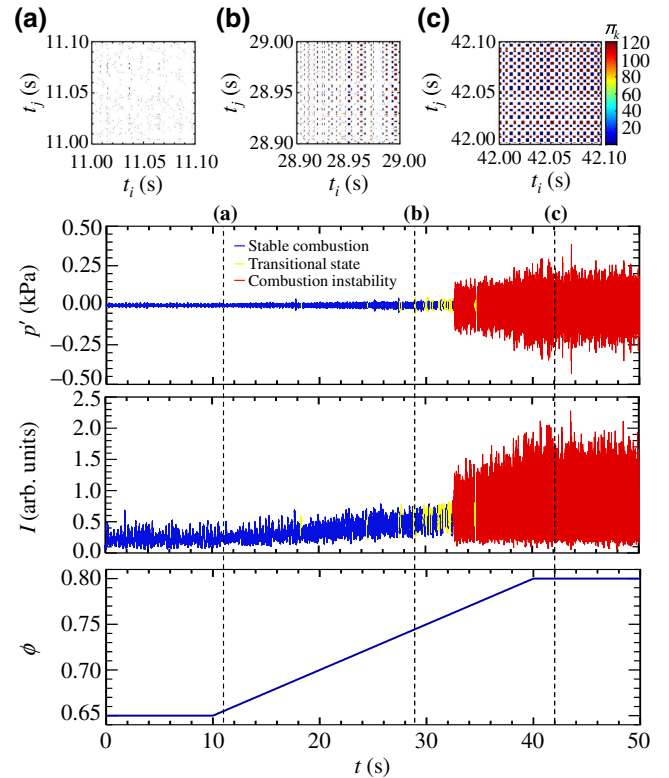

FIG. 5. Variations in the acoustic pressure fluctuations p' and heat release rate I with increasing equivalence ratio ϕ as a function of time t for test data using the trained CNN. Here, (a) $t = 11.1$ s, (b) $t = 29.0$ s, and (c) $t = 42.1$ s.
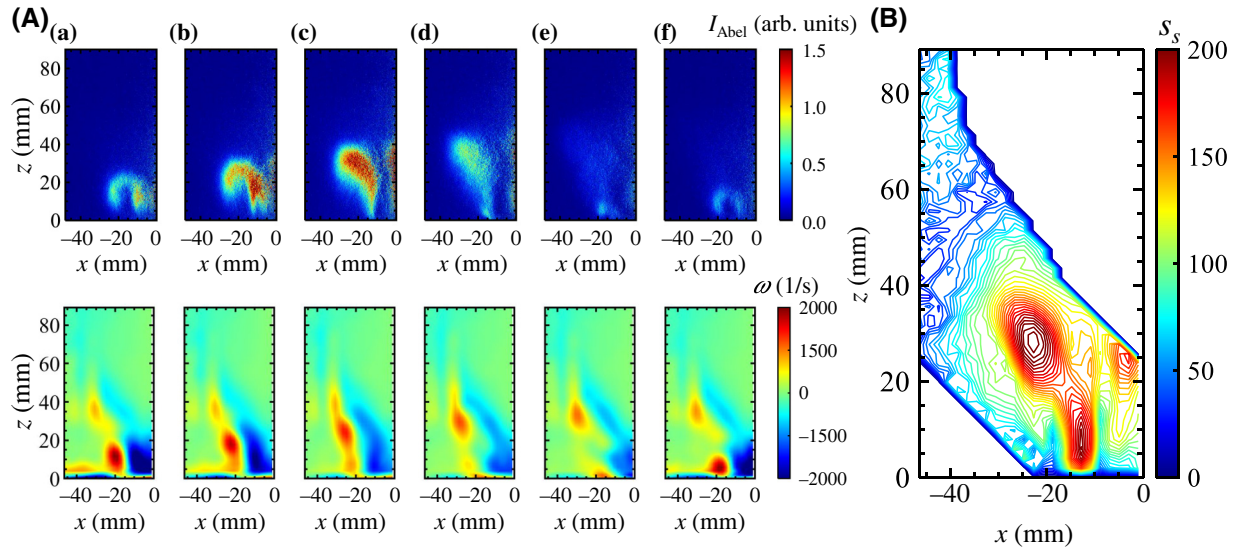
FIG. 6. (A) Spatial distribution of the phase-locked OH* chemiluminescence intensity and vorticity fields. (B) Distribution of the vertex strength s_s in a weighted spatial network. Here, (a) phase angle $\theta = 0°$, (b) $\theta = 60°$, (c) $\theta = 120°$, (d) $\theta = 180°$, (e) $\theta = 240°$, and (f) $\theta = 300°$.

important for building a precursor detector of combustion instability from the viewpoint of practical applications. A convolutional recurrent neural network has more recently been utilized for an early detection of combustion instability in a different type of swirl-stabilized combustor [53] from our combustor. In addition to a recent study [53], our methodology using deep learning has potential use in detecting a precursor of combustion instability.

Figure 6 shows the phase-locked OH* chemiluminescence intensity and vorticity fields during combustion instability at $\phi = 0.8$, together with the distribution of the vertex strength s_s in the weighted spatial network. Here, the OH* chemiluminescence intensity field is obtained by inverse Abel transformation, and the local maximum (minimum) of p' corresponds to the phase angle $\theta = 90°$ $(270°)$. A transverse vortex begins to be induced near the inlet of the combustor at $\theta = 300°$. The OH* chemiluminescence intensity significantly increases with the downstream movement of the vortex along the shear layer region between the IRF and the ORF. The region of high OH* chemiluminescence intensity expands at the location where a flame front is rolled up by the development of the vortical structure at $\theta = 120°$. We clearly observe that s_s takes high values at $z \sim 30$ mm in the shear layer region. These results show that a strong mutual coupling between heat release rate and flow velocity fluctuations occurs near the location of the rolled-up flame front owing to the developed large-scale transverse vortex.

Figure 7(A) shows time variations in p', I', and the cluster coefficient $\langle c \rangle$ in the thermoacoustic power network during one cycle of combustion instability at $\phi = 0.8$. Here, these quantities are normalized by their maximum

values. We observe a gradual increase in $\langle c \rangle$ when p' and I' increase from $t = 524.7$ to 526 ms. $\langle c \rangle$ notably increases when p' and I' decrease from $t = 527.5$ to 529 ms. The important point is that $\langle c \rangle$ takes a higher value at $t \sim$ 529 ms [see Fig. 7(f)] than at $t \sim 526$ ms [see Fig. 7(c)]. This shows that the connection of all the nodes in the thermoacoustic power network is heterogeneous at $t \sim$ 526 ms, whereas the entire network structure is highly clustered and homogeneously connected at $t \sim 529$ ms. The spatial distributions of the vertex strength s_a corresponding to (a)–(f) in Fig. 7(A) are shown in Fig. 7(B). When p' and I' nearly take the local maximum at $t = 526.3$ ms, a high region of s_a is locally formed at 20 mm $< z <$ 40 mm. Here s_a decreases with time in response to the decrease in both p' and I'. These results indicate that the thermoacoustic power driving combustion instability is produced by the mutual interaction between acoustic pressure and heat release rate fluctuations near their local maximum. As is shown in Fig. 6, high vertex strength in the spatial network constructed from I' and u' appears at $z \sim 30$ mm corresponding to the location of the rolled-up flame front in the shear layer region. On these bases, local thermoacoustic cluster is produced by the rolled-up flame front owing to the developed large-scale transverse vortical structure. We here note that a local high s_a is not formed at $t = 529.2$ ms, which shows that at the time when both p' and I' decrease, the vortical structure does not produce thermoacoustic power source clusters. Temporal evolution of the community structure in the turbulence network is shown in Fig. 7(C), together with the hub obtained by the module degree. Here, the width of the black line represents the degree of interaction between communities. When p' and
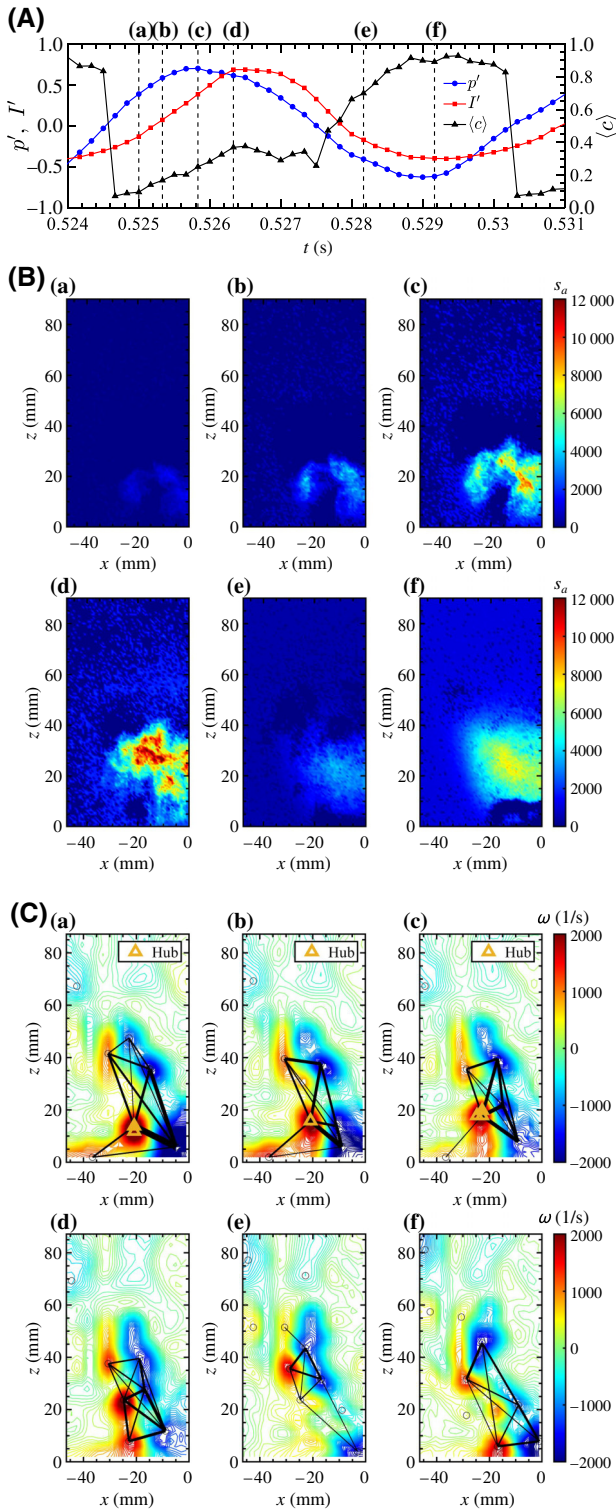
FIG. 7. (A) Time variations in the acoustic pressure fluctuations p', heat release rate fluctuations I', and cluster coefficient $\langle c \rangle$ in the thermoacoustic power network over one cycle of combustion instability. (B) Spatial distribution of the vertex strength s_a in the thermoacoustic power network. (C) Community structure in the turbulence network. Here, (a) $t = 525$ ms, (b) $t = 525.3$ ms, (c) $t = 525.8$ ms, (d) $t = 526.3$ ms, (e) $t = 528.2$ ms, and (f) $t = 529.2$ ms.
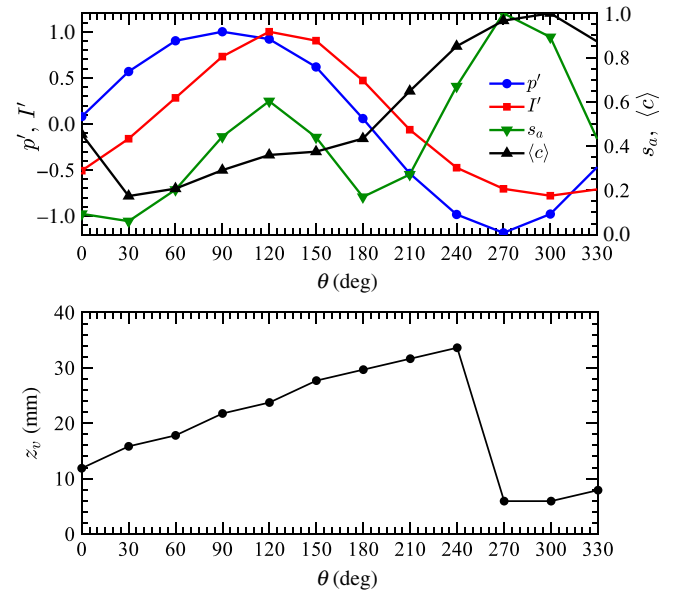

FIG. 8. Variations in the phase-locked acoustic pressure fluctuations p', heat release rate fluctuations I', vertex strength s_a, and the cluster coefficient $\langle c \rangle$ in the thermoacoustic power network, and the distance between the nozzle exit and the center of the transverse vortex z_v during combustion instability with respect to the phase angle θ.

I' increase from $t = 525$ to 526 ms, the connection with other communities is strengthen with the movement of the transverse vortex, forming a primary hub. In contrast, the hub is lost when they decrease from $t = 526.3$ to 529.2 ms, resulting in the attenuation of thermoacoustic power source clusters. These results show that the extraction of thermoacoustic power source clusters, community structure and hub locations comprehensively clarify the mutual coupling during combustion instability in a swirl-stabilized turbulent combustor. Figure 8 shows the variations in the phase-locked p', I', s_a, $\langle c \rangle$, and z_v in terms of θ. Here, z_v is the distance between the nozzle exit and the center of the transverse vortex. We observe the phase difference between p' and I' with $\theta = 30°$. s_a takes a local maximum at $\theta = 120°$ and $270°$. These results show that acoustic energy is amplified in the duration between $\theta = 120°$ and $270°$. Here $\langle c \rangle$ takes a low value in the range of $\theta = 30°$ and $150°$ forming locally strong thermoacoustic power sources, whereas it takes a local maximum at $\theta = 270°$ forming widely distributed thermoacoustic power sources. Here z_v ranges from 15 to 30 mm at $30° < \theta < 150°$, which demonstrates that the flame front is suck in by the traveling transverse vortex, resulting in the local formation of strong thermoacoustic power sources.

Figure 9 shows the variation in the transfer entropy S_T at a representative location in the shear layer region during combustion instability at $\phi = 0.8$, together with the spatial-network-based transfer entropy E_T. Here, $(x, z) = (-22.7$ mm, 25.7 mm$)$. Note that we use the transfer
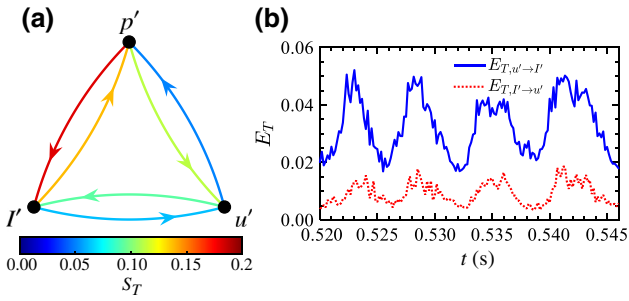
FIG. 9. Variation in the transfer entropy S_T at a representative location in the shear layer region during combustion instability, together with the temporal evolution of the spatial-network-based transfer entropy E_T. Here, $(x, z) = (-22.7 \text{ mm}, 25.7 \text{ mm})$.

entropy [47] for the estimation of S_T. Here $S_{T,p'\to I'}$ is larger than $S_{T,I'\to p'}$, which indicates that the acoustic pressure fluctuations relatively affect the heat release rate fluctuations during well-developed combustion instability; $S_{T,p'\to u'}$ is larger than $S_{T,u'\to p'}$, indicating that the acoustic pressure fluctuations relatively affect the flow velocity fluctuations; and $S_{T,u'\to I'}$ is larger than $S_{T,I'\to u'}$. An important result is that $E_{T,u'\to I'}$ is larger than $E_{T,I'\to u'}$ as well as the relationship between $S_{T,u'\to I'}$ and $S_{T,I'\to u'}$. Here $E_{T,u'\to I'}$ and $E_{T,I'\to u'}$ periodically fluctuate with the same frequency as that of the dominant mode in pressure fluctuations. These results suggest the two important points concerning the feedback process during combustion instability: (i) the large pressure fluctuations contribute to the periodic formation of the large-scale transverse vortex in response to the 1/4 longitudinal acoustic mode of the combustor and (ii) the flow velocity fluctuations due to the developed transverse vortex deforming the flame front lead to large heat release rate fluctuations in the shear layer region. Godavarthi *et al.* [8] have adopted a different class of causality analysis incorporating complex-network- and recurrence-based approaches for combustion instability in a bluff-body-type turbulent combustor. The causality analysis has also been used for clarifying the synchronization between acoustic pressure fluctuations in multiple coupled combustors [5]. In addition to the causality analysis [8], the spatial-network-based transfer entropy we proposed here is also a useful causality index and will be helpful for understanding the feedback coupling between the fluctuations in the flow velocity and heat release rate fields during combustion instability. In this work, we have focused on obtaining a comprehensive understanding of the feedback coupling during combustion instability, including an early detection methodology for combustion instability using deep learning. The importance of the directional coupling from flow velocity to heat release rate fluctuations in the shear layer from the viewpoint of complex-systems approach has not been clarified experimentally in previous studies on the feedback process during combustion instability in various turbulent combustors.

V. SUMMARY

We have experimentally studied the feedback coupling of thermoacoustic combustion instability in a swirl-stabilized turbulent combustor from the viewpoint of complex-systems approach based on information theory, symbolic dynamics, and complex network, including an early detection of combustion instability by a CNN using deep learning. We have conducted the simultaneous measurement of acoustic pressure, heat release rate, and flow velocity fluctuations during combustion instability.

The rolled-up flame front due to an upward traveling of a large-scale transverse vortex gives rise to large heat release rate fluctuations in the shear layer region between the IRF and the ORF. This is clearly shown by the appearance of a strong correlation between the heat release rate and flow velocity fluctuations in a weighted spatial network. The vertex strength and cluster coefficient in a thermoacoustic power network show that a large-scale thermoacoustic power source cluster is formed as the acoustic pressure and heat release rate fluctuations take a local maximum. The module degree in the turbulence network shows that the primary hub of the communities in the network is formed with temporal enhancement of both acoustic pressure and heat release rate fluctuations. The large pressure fluctuations contribute significantly to the periodic formation of the transverse vortex in response to the 1/4 longitudinal acoustic mode of the combustor, which is identified by the transfer entropy between the acoustic pressure and flow velocity fluctuations. The directional coupling from flow velocity to heat release rate fluctuations clearly appears near the location of the rolled-up flame front. This is reasonably demonstrated by a spatial-network-based transfer entropy we proposed in this study. These physical processes fulfill an important role in the formation of a strong and local thermoacoustic power source cluster during combustion instability.

A two-dimensional plane, which consists of the transition network entropy and the symbolic recurrence rate constructed from the pressure and heat release rate fluctuations, can capture a significant change in combustion state from stable combustion to combustion instability. SRPs correlated with the two-dimensional clustering plane obtained by the k-means method, which is learned by a CNN, enable us to detect a precursor of combustion instability.

ACKNOWLEDGMENTS

[1] T. C. Lieuwen, *Unsteady Combustor Physics* (Cambridge University Press, Cambridge, 2012).

[2] R. I. Sujith and V. R. Unni, Complex system approach to investigate and mitigate thermoacoustic instability in turbulent combustors, Phys. Fluids **32,** 061401 (2020).

[3] I. Pavithran, V. R. Unni, and R. I. Sujith, Critical transitions and their early warning signals in thermoacoustic systems, Eur. Phys. J. Spec. Top. **230,** 3411 (2021).

[4] R. I. Sujith and S. A. Pawar, *Thermoacoustic Instability* (Springer Nature, London, 2021).

[5] Y. Guan, K. Moon, K. T. Kim, and L. K. B. Li, Synchronization and chimeras in a network of four ring-coupled thermoacoustic oscillators, J. Fluid Mech. **938,** A5 (2022).

[6] S. A. Pawar, A. Seshadri, V. R. Unni, and R. I. Sujith, Thermoacoustic instability as mutual synchronization between the acoustic field of the confinement and turbulent reactive flow, J. Fluid Mech. **827,** 664 (2017).

[7] S. Mondal, V. R. Unni, and R. I. Sujith, Onset of thermoacoustic instability in turbulent combustors: an emergence of synchronized periodicity through formation of chimera-like states, J. Fluid Mech. **811,** 659 (2017).

[8] V. Godavarthi, S. A. Pawar, V. R. Unni, R. I. Sujith, N. Marwan, and J. Kurths, Coupled interaction between unsteady flame dynamics and acoustic field in a turbulent combustor, Chaos **28,** 113111 (2018).

[9] Y. Guan, L. K. B. Li, B. Ahn, and K. T. Kim, Chaos, synchronization, and desynchronization in a liquid-fueled diffusion-flame combustor with an intrinsic hydrodynamic mode, Chaos **29,** 053124 (2019).

[10] J. M. Amigó, *Permutation Complexity in Dynamical Systems* (Springer Berlin, Heidelberg, 2010).

[11] H. Gotoda, M. Amano, T. Miyano, T. Ikawa, K. Maki, and S. Tachibana, Characterization of complexities in combustion instability in a lean premixed gas-turbine model combustor, Chaos **22,** 043128 (2012).

[12] Y. Okuno, M. Small, and H. Gotoda, Dynamics of self-excited thermoacoustic instability in a combustion system: pseudo-periodic and high-dimensional nature, Chaos **25,** 043107 (2015).

[13] J. Tony, E. A. Gopalakrishnan, E. Sreelekha, and R. I. Sujith, Detecting deterministic nature of pressure measurements from a turbulent combustor, Phys. Rev. E **92,** 062902 (2015).

[14] H. Kobayashi, H. Gotoda, S. Tachibana, and S. Yoshida, Detection of frequency-mode-shift during thermoacoustic combustion oscillations in a staged aircraft engine model combustor, J. Appl. Phys. **122,** 224904 (2017).

[15] Y. Guan, M. Murugesan, and L. K. B. Li, Strange nonchaotic and chaotic attractors in a self-excited thermoacoustic oscillator subjected to external periodic forcing, Chaos **28,** 093109 (2018).

[16] C. Bandt and B. Pompe, Permutation Entropy: a Natural Complexity Measure for Time Series, Phys. Rev. Lett. **88,** 174102 (2002).

[17] M. Small, Complex networks from time series: Capturing dynamics, IEEE Int. Symp. Circuits Syst., 2509 (2013).

[18] M. McCullough, M. Small, T. Stemler, and H. H.-C. Iu, Time lagged ordinal partition networks for capturing dynamics of continuous dynamical systems, Chaos **25,** 053101 (2015).

[19] H. Kobayashi, H. Gotoda, and S. Tachibana, Nonlinear determinism in degenerated combustion instability in a gas-turbine model combustor, Phys. A **510,** 345 (2018).

[20] C. Aoki, H. Gotoda, S. Yoshida, and S. Tachibana, Dynamic behavior of intermittent combustion oscillations in a model rocket engine combustor, J. Appl. Phys. **127,** 224903 (2020).

[21] K. Asami, T. Kawada, S. Kishiya, and H. Gotoda, Dynamic behavior and driving region of thermoacoustic combustion oscillations in a swirl-stabilized turbulent combustor, Europhys. Lett. **139,** 13001 (2022).

[22] N. Marwan, M. C. Romano, M. Thiel, and J. Kurths, Recurrence plots for the analysis of complex systems, Phys. Rep. **438,** 237 (2007).

[23] T. Hachijo, S. Masuda, T. Kurosaka, and H. Gotoda, Early detection of thermoacoustic combustion oscillations using a methodology combining statistical complexity and machine learning, Chaos **29,** 103123 (2019).

[24] Y. Shinchi, N. Takeda, H. Gotoda, T. Shoji, and S. Yoshida, Early detection of thermoacoustic combustion oscillations in staged multisector combustor, AIAA J. **59,** 4086 (2021).

[25] G. Waxenegger-Wilfing, U. Sengupta, J. Martin, W. Armbruster, J. Hardi, M. Juniper, and M. Oschwald, Early detection of thermoacoustic instabilities in a cryogenic rocket thrust chamber using combustion noise features and machine learning, Chaos **31,** 063128 (2021).

[26] O. A. Rosso, H. A. Larrondo, M. T. Martin, A. Plastino, and M. A. Fuentes, Distinguishing Noise from Chaos, Phys. Rev. Lett. **99,** 154102 (2007).

[27] V. N. Vapnik, An overview of statistical learning theory, IEEE Trans. Neural Networks **10,** 988 (1999).

[28] C. M. Bishop, *Pattern Recognition and Machine Learning* (Springer-Verlag, Berlin, 2006).

[29] T. Hashimoto, H. Shibuya, H. Gotoda, Y. Ohmichi, and S. Matsuyama, Spatiotemporal dynamics and early detection of thermoacoustic combustion instability in a model rocket combustor, Phys. Rev. E **99,** 032208 (2019).

[30] J. Zhang, J. Zhou, M. Tang, H. Guo, M. Small, and Y. Zou, Constructing ordinal partition transition networks from multivariate time series, Sci. Rep. **7,** 7795 (2017).

[31] Y. LeCun, B. Boser, J. S. Denker, D. Henderson, R. E. Howard, W. Hubbard, and L. D. Jackel, Backpropagation applied to handwritten zip code recognition, Neural Comput. **1,** 541 (1989).

[32] Y. LeCun, L. Bottou, Y. Bengio, and P. Haffner, Gradient-based learning applied to document recognition, Proc. IEEE **86,** 2278 (1998).

[33] E. A. Ruiz, V. R. Unni, I. Pavithran, R. I. Sujith, and A. Saha, Convolutional neural networks to predict the onset of oscillatory instabilities in turbulent systems, Chaos **31,** 093131 (2021).

[34] S. Murayama, H. Kinugawa, I. T. Tokuda, and H. Gotoda, Characterization and detection of thermoacoustic combustion oscillations based on statistical complexity and complex-network theory, Phys. Rev. E **97,** 022223 (2018).

[35] G. Iacobello, S. Scarsoglio, J. G. M. Kuerten, and L. Ridolfi, Spatial characterization of turbulent channel flow via complex networks, Phys. Rev. E **98,** 013107 (2018).

[36] Y. Ozaki, K. Kawano, and H. Gotoda, Gravitational effect on the nonlinear dynamics of a buoyant turbulent flame, Chaos **32**, 083147 (2022).

[37] A. Krishnan, R. I. Sujith, N. Marwan, and J. Kurths, On the emergence of large clusters of acoustic power sources at the onset of thermoacoustic instability in a turbulent combustor, J. Fluid Mech. **874**, 455 (2019).

[38] S. Shima, K. Nakamura, H. Gotoda, Y. Ohmichi, and S. Matsuyama, Formation mechanism of high-frequency combustion oscillations in a model rocket engine combustor, Phys. Fluids **33**, 064108 (2021).

[39] P. Holme, S. M. Park, B. J. Kim, and C. R. Edling, Korean university life in a network perspective: Dynamics of a large affiliation network, Phys. A **373**, 821 (2007).

[40] K. Taira, A. G. Nair, and S. L. Brunton, Network structure of two-dimensional decaying isotropic turbulence, J. Fluid Mech. **795**, R2 (2016).

[41] S. Murayama and H. Gotoda, Attenuation behavior of thermoacoustic combustion instability analyzed by a complex-network-and synchronization-based approach, Phys. Rev. E **99**, 052222 (2019).

[42] T. Kurosaka, S. Masuda, and H. Gotoda, Attenuation of thermoacoustic combustion oscillations in a swirl-stabilized turbulent combustor, Chaos **31**, 073121 (2021).

[43] A. Krishnan, R. I. Sujith, N. Marwan, and J. Kurths, Suppression of thermoacoustic instability by targeting the hubs of the turbulent networks in a bluff body stabilized combustor, J. Fluid Mech. **916**, A20 (2021).

[44] V. D. Blondel, J.-L. Guillaume, R. Lambiotte, and E. Lefebvre, Fast unfolding of communities in large networks, J. Stat. Mech. **2008,** P10008 (2008).

[45] R. Guimera and L. A. N. Amaral, Functional cartography of complex metabolic networks, Nature **433**, 895 (2005).

[46] S. Balusamy, L. K. B. Li, Z. Han, M. P. Juniper, and S. Hochgreb, Nonlinear dynamics of a self-excited thermoacoustic system subjected to acoustic forcing, Proc. Combust. Inst. **35**, 3229 (2015).

[47] T. Schreiber, Measuring Information Transfer, Phys. Rev. Lett. **85**, 461 (2000).

[48] M. V. Caballero-Pintado, M. Matilla-García, and M. Ruiz Marín, Symbolic recurrence plots to analyze dynamical systems, Chaos **28**, 063112 (2018).

[49] P. Kim, *MATLAB Deep Learning* (Apress, Seoul, 2017).

[50] D. E. Rumelhart and J. L. McClelland, PDP Research Group, *Parallel Distributed Processing: Explorations in the Microstructure of Cognition, Vol. 1: Foundations* (MIT Press, 1986).

[51] T. Kobayashi, S. Murayama, T. Hachijo, and H. Gotoda, Early Detection of Thermoacoustic Combustion Instability using a Methodology Combining Complex Networks and Machine Learning, Phys. Rev. Appl. **11**, 064034 (2019).

[52] J. Eckmann, S. O. Kamphorst, and D. Ruelle, Recurrence plots of dynamical systems, Europhys. Lett. **4**, 973 (1987).

[53] A. Cellier, C. J. Lapeyre, G. Öztarlik, T. Poinsot, T. Schuller, and L. Selle, Detection of precursors of combustion instability using convolutional recurrent neural networks, Combust. Flame **233**, 111558 (2021).